MRI-coupled fluorescence tomography of murine glioma metabolic activity

Scott C. Davis[1], Summer L. Gibbs-Strauss[1], Hamid Dehghani[2], Brian W. Pogue[1], and Keith D. Paulsen[1]
[1] Thayer School of Engineering, Dartmouth College, Hanover NH 03755
[2] School of Physics, University of Exeter, UK
(Email: scott.c.davis@dartmouth.edu, Tel:(603) 650-3561, Fax:(603) 646-3856)

Abstract: Protoporphyrin IX fluorescence activity in mouse model gliomas is imaged in nude mice using an MRI-coupled spectroscopy scanner. Segmented MR images acquired simultaneously with fluorescence spectra are used to guide fluorescence yield reconstruction.

OCIS codes: (170.0110) Imaging Systems; (170.3880) Medical and biological imaging; (170.6280) Spectroscopy, fluorescence and luminescence; (170.6960) Tomography

1. Introduction

Imaging fluorescence activity of molecular probes live small animals has broad implications for disease research and therapy development. Though commonly used, fluorescence scanners for in vivo imaging in the planar geometry produce severely surface-weighted images with little sensitivity to deeper lesions due to the nature of optical photon propagation in tissue. Fluorescence tomography was developed to address this problem by modeling the photon propagation (often as a diffusion process) in tissue and the development of several scanners to collect the requisite imaging data has been reported [1-6]. Unfortunately, the highly scattered photon field and under-determined nature of the optical problem limits the spatial resolution, and therefore quantitative accuracy, of fluorescence activity images reconstructed using these model based approaches. This is also true for the closely related diffuse optical tomography (DOT), of which fluorescence diffuse tomography is a subset; however, researchers in the DOT field have found that incorporating tissue structure determined from highly resolved clinical imaging modalities dramatically improves DOT images [7-10]. Similar imaging improvements have recently been shown for fluorescence tomography [11] for tissue phantoms, but no in vivo data has been published to date.

In this study, a newly developed MR-coupled spectroscopy imaging system is used to demonstrate fluorescence activity imaging of a metabolically targeted fluorescence contrast agent in vivo. Protoporphyrin IX (PPIX) is an endogenous fluorophore commonly targeted for photodynamic therapy. It is an intermediary product in the heme biosynthesis pathway, a process which can be overloaded upon the administration of the pro-drug Aminoaluvelinic Acid (ALA) (Fisher Scientific Inc.) resulting in the buildup of PPIX in metabolically overactive cells, such as found in malignant pathologies. ALA can produce PPIX tumor-to-healthy tissue contrasts of up to 10:1 in brain tumors and is used here for imaging gliomas in nude mice.

2. Methods

The 3T MRI-coupled spectroscopy system is show in Fig. 1 and consists of sixteen Princeton Instruments/Acton Insight:400F Integrated Spectrometers (Acton, MA) which use Pixis CCD cameras cooled to -70 C. Ports in the wall of the magnet bore room provide access for long silica fibers to couple light between the animal surface and spectroscopic detectors. The fibers operate in contact mode and couple light emitted from the tissue surface, through an automated filter wheel, and into the spectrometer slit. The animal interface is a custom designed rodent MRI coil (Philips , Hamburg, DE) with access holes in one plane to accommodate up to 16 fibers in a circular array.

Nine-L glioma models were implanted intracranially in nude mice and fluorescence imaging began two weeks after implantation. The pro-drug Aminolevulinic acid (ALA) was injected and allowed to incubate for two hours prior to image acquisition, a time interval found to be optimal for PPIX buildup in previous studie. Four source/detector fiber positions were used for a total of 12 emission spectra, though the coil system is capable of accommodating all 16 channels. MRI images acquired included standard T2 weighted and T1 weighted with gadolinium contrast, and fluorescence emission and excitation transmission measurements were collected while the MR acquisition was underway.

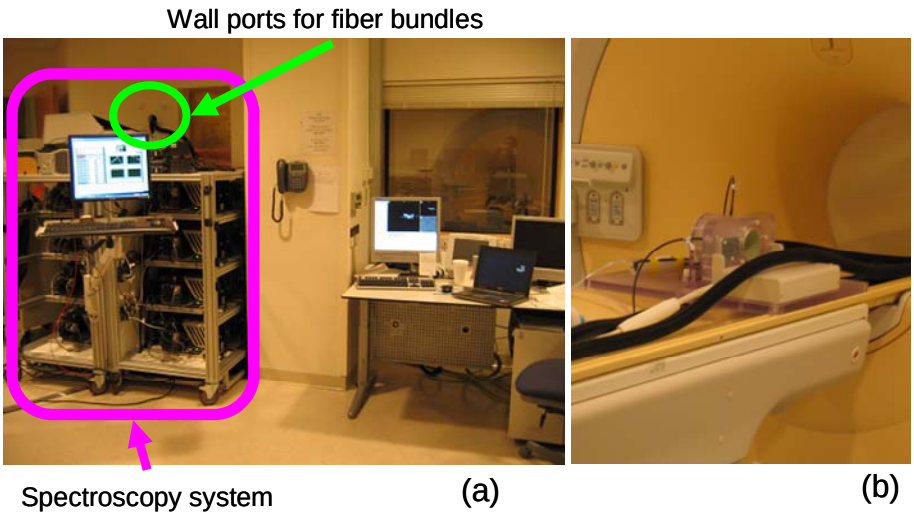

Fig. 1. The spectroscopic detection system is built on carts to allow positioning the MRI control room (a). Ports in the wall leading to the magnet room provide fiber bundle access into the MRI bore. The animal coil, depicted in (b), accommodates up to 16 spectroscopy fibers.

PPIX absorbs strongly at 635nm and has an emission peak at approximately 705nm. In this study a 635nm excitation source was used to excite the tissue and a 650nm long pass interference filter (Omega Optics, Brattelboro, VT) provided over 5OD excitation rejection before the measure light entered the spectrometer. Despite this, fluorescence emission data is composed of excitation cross-talk and the fluorescence emission peak. A least squares spectral fitting algorithm was used to process each spectrum and de-convolve the spectral components. The isolated fluorescence emission peak was integrated and scaled using the transmission measurements recorded with the excitation laser source. Relative fluorescence intensities determined in this manner serve as the calibrated data set for image reconstruction.

Images of PPIX fluorescence yield are recovered using a diffuse optical fluorescence tomography technique assisted by the simultaneously acquired MRI images. Coronal images of the mouse head were used to identify the optical imaging plane defined by the fiber bundles. Image intensity thresholds were used to delineate the outer boundary of the mouse domain as well as segment internal features of the tissue. Finite element meshes were automatically generated from the segmented images, preserving the outer boundary and internal features defined in the segmentation. The parameter update of fluorescence yield is given by

$$\Delta\eta\mu_{af} = \left[J^T J + \beta L^T L\right]^{-1} J^T \left(\Phi_m^{Meas} - \Phi_m^C\right)$$

where fluorescence yield is the product of the fluorophore's quantum yield, η, and its absorption coefficient, $\mu_{af}(r)$, J is the Jacobian matrix describing the sensitivity of boundary data to the parameter of interest and β is a fixed fraction multiplied by the maximum value on the diagonal of J^TJ. Spatial prior information is introduced in the dimensionless 'filter' matrix, L, which encodes different anatomical regions defined by the MRI segmentation. In this case, a simple two-region (tumor and healthy) segmentation was used. Values for the background optical properties were assigned manually, but may be using a PMT-based frequency domain system currently being integrated into the spectroscopic fiber coupling array.

3. Results

A recovered image of PPIX fluorescence yield is presented in figure 2. A coronal slice from the MRI images was used to segment the imaging volume and delineate the tumor region (white regions in the lower left corner of the domain) from the rest of the tissue volume. A two-region soft spatial priors approach was used to guide the fluorescence image reconstruction algorithm. The resulting image shows elevated fluorescence activity in the tumor region compared to the rest of the imaging domain.

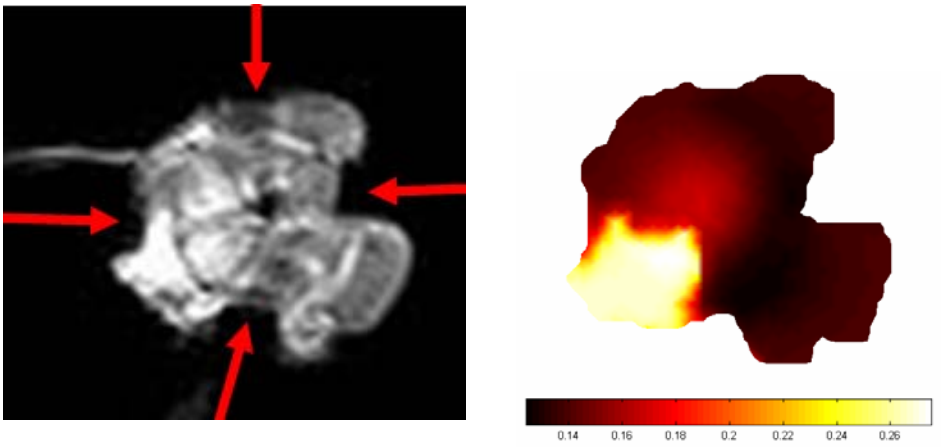

Fig. 2. In this pilot study, four source/detector fibers were used to acquire fluorescence emission spectra. A segmented MRI image is used to mesh the tissue slice for DOFT reconstructions. Recovered fluorescence yield images show elevated PPIX fluorescence in the tumor region.

4. Discussion

A pilot study in nude mice demonstrates the feasibility of using spatial prior information from MRI images for in vivo imaging of fluorescence yield. MRI spatial guidance provided the anatomical template upon which fluorescence activity is quantified, even with sparse data as demonstrated in this case. An imminent study is exploring how the algorithm handles incorrectly identified tissue regions based on false positive or false negative MRI results.

The spectroscopic detection system is flexible in terms of its ability to image a wide array of NIR fluorophores. It is also capable of MRI- coupled spectrally resolved broadband transmission tomography and bioluminescence tomography.

5. Acknowledgements

This work was funded by the National Institutes of Health grants RO1 CA109558, RO1 CA69544, U54 CA105480, Philips Research Hamburg, as well as Department of Defense Breast Cancer pre-doctoral fellowship BC051058.

6. References

1. N. Deliolanis, T. Lasser, D. Hyde, A. Soubret, J. Ripoll, and V. Ntziachristos, "Free-space fluorescence molecular tomography utilizing 360 degree geometry prejections," Optics Letters **32**, 382-384 (2007).
2. H. Meyer, A. Garofalakis, G. Zacharakis, S. Psycharakis, C. Mamalaki, D. Kioussis, E. N. Economou, V. Ntziachristos, and J. Ripoll, "Noncontact optical imaging in mice with full angular coverage and automatic surface extraction," Applied Optics **46**, 3617-3627 (2007).
3. S. V. Patwardhan, S. R. Bloch, S. Achilefu, and J. P. Culver, "Time-dependent whole-body fluorescence tomography of probe bio-distribution in mice," Opt. Exp. **13**, 2564-2577 (2005).
4. J. Ripoll, R. B. Schulz, and V. Ntziachristos, "Free-space propagation of diffuse light: theory and experiments," Physical Review Letters **91**, 5 (2003).
5. R. B. Schulz, J. Ripoll, and V. Ntziachristos, "Experimental fluorescence tomography of tissues with noncontact measurements," IEEE Transactions on Medical Imaging **23**, 492-500 (2004).
6. G. Zacharakis, J. Ripoll, R. Weissleder, and V. Ntziachristos, "Fluorescent protein tomography scanner for small animal imaging," IEEE Transactions on Medical Imaging **24**, 878-885 (2005).
7. B. Brooksby, S. Jiang, C. Kogel, M. Doyley, H. Dehghani, J. B. Weaver, S. P. Poplack, B. W. Pogue, and K. D. Paulsen, "Magnetic resonance-guided near-infrared tomography of the breast," Rev. Sci. Instrum. **75**, 5262-5270 (2004).
8. M. Guven, B. Yazici, X. Intes, and B. Chance, "Diffuse optical tomography with a priori anatomical information," Phys. Med. Biol. **50**, 2837-2858 (2005).
9. X. Intes, C. Maloux, M. Guven, B. Yazici, and B. Chance, "Diffuse Optical tomography with physiological and spatial a priori constraints," Phys. Med. Biol. **49**, N155-N163 (2004).
10. G. Zacharakis, H. Kambara, H. A. Shih, J. Ripoll, J. Grimm, Y. Saekl, R. Weissleder, and V. Ntziachristos, "Volumetric tomography of fluorescent protiens through small animals in vivo," Proceedings of the National Academy of Sciences of the United States of America **102**, 18252-18257 (2005).
11. S. C. Davis, H. Dehghani, J. Wang, S. Jiang, B. W. Pogue, and K. D. Paulsen, "Image-guided diffuse optical fluorescence tomography implemented with Laplacian-type regularization," Optics Express **15**, 4066-4082 (2007).